

## Structures and magnetic properties of $\text{CrSi}_n^-$ ( $n = 3-12$ ) clusters: Photoelectron spectroscopy and density functional calculations

Xiangyu Kong, Hong-Guang Xu, and Weijun Zheng

Citation: *J. Chem. Phys.* **137**, 064307 (2012); doi: 10.1063/1.4742065

View online: <http://dx.doi.org/10.1063/1.4742065>

View Table of Contents: <http://jcp.aip.org/resource/1/JCPSA6/v137/i6>

Published by the [American Institute of Physics](#).

---

### Additional information on *J. Chem. Phys.*

Journal Homepage: <http://jcp.aip.org/>

Journal Information: [http://jcp.aip.org/about/about\\_the\\_journal](http://jcp.aip.org/about/about_the_journal)

Top downloads: [http://jcp.aip.org/features/most\\_downloaded](http://jcp.aip.org/features/most_downloaded)

Information for Authors: <http://jcp.aip.org/authors>

## ADVERTISEMENT



**AFM-RAMAN** **BRUKER**

LEADING PERFORMANCE  
WIDEST PRODUCT RANGE

[www.bruker-axs.com](http://www.bruker-axs.com)

CLICK TO REQUEST INFO

# Structures and magnetic properties of $\text{CrSi}_n^-$ ( $n = 3-12$ ) clusters: Photoelectron spectroscopy and density functional calculations

Xiangyu Kong, Hong-Guang Xu, and Weijun Zheng<sup>a)</sup>

Beijing National Laboratory for Molecular Sciences, State Key Laboratory of Molecular Reaction Dynamics, Institute of Chemistry, Chinese Academy of Sciences, Beijing 100190, China

(Received 16 May 2012; accepted 19 July 2012; published online 8 August 2012)

Chromium-doped silicon clusters,  $\text{CrSi}_n^-$  ( $n = 3-12$ ), were investigated with anion photoelectron spectroscopy and density functional theory calculations. The combination of experimental measurement and theoretical calculations reveals that the onset of endohedral structure in  $\text{CrSi}_n^-$  clusters occurs at  $n = 10$  and the magnetic properties of the  $\text{CrSi}_n^-$  clusters are correlated to their geometric structures. The most stable isomers of  $\text{CrSi}_n^-$  from  $n = 3$  to 9 have exohedral structures with magnetic moments of  $3-5\mu_B$  while those of  $\text{CrSi}_{10}^-$ ,  $\text{CrSi}_{11}^-$ , and  $\text{CrSi}_{12}^-$  have endohedral structures and magnetic moments of  $1\mu_B$ . © 2012 American Institute of Physics. [<http://dx.doi.org/10.1063/1.4742065>]

## I. INTRODUCTION

Introducing of transition metal atoms into silicon clusters may stabilize their cage structures, therefore, allows them to be used as building blocks for novel nanomaterials.<sup>1</sup> On account of their potential applications in nanomaterials and semiconductors, transition metal-doped silicon clusters have been studied extensively by experiments<sup>2-19</sup> and theoretical calculations<sup>20-50</sup> in the last decades.

Chromium, silicon, and their alloys are very important materials in the manufacture of thin film resistors and microelectronic devices.<sup>51-54</sup> It has been suggested that chromium silicide is a potentially important contact material in future nanosystems because chromium silicide nanostructures can reduce the energy barrier between the metal and semiconductor layers.<sup>55</sup> Chromium-doped silicon clusters have been studied by many researchers. Beck conducted the first mass spectrometry study of  $\text{MSi}_n^+$  ( $M = \text{Cr}, \text{Mo}$  and  $\text{W}$ ) clusters and found that  $\text{CrSi}_n^+$  with  $n = 15$  and 16 have the most intense peaks in the mass spectra.<sup>2,3</sup> Han *et al.*<sup>38,56</sup> investigated the structures of  $\text{CrSi}_n$  ( $n = 1-6, n = 15$ ) clusters by theoretical calculations. Lau *et al.*<sup>15</sup> studied  $\text{MSi}_{16}^+$  ( $M = \text{Ti}, \text{V}$  and  $\text{Cr}$ ) clusters using x-ray absorption spectroscopy and revealed that Cr atoms can impose a geometric rearrangement in silicon clusters and the highly symmetric silicon cage can affect the electronic structure of Cr atom. Khanna *et al.*<sup>23</sup> conducted theoretical calculations on  $\text{CrSi}_n$  ( $n = 11-14$ ) clusters and showed that  $\text{CrSi}_{12}$  has a  $D_{6h}$  endohedral structure. Although it has been shown that  $\text{CrSi}_n$  is able to form endohedral structure at large cluster size, it is still in question regarding the onset size of endohedral structures. The theoretical calculations of Han and Hagelberg<sup>38</sup> found an  $O_h$  symmetry endohedral structure for neutral  $\text{CrSi}_6$ . While Kawamura *et al.*<sup>57</sup> suggest that the Cr atom is not fully surrounded by Si atoms at  $n = 8-11$  and the cage is not completely formed until  $n = 12$ . On the other hand, Bowen and co-workers<sup>6</sup> measured photo-

electron spectra of  $\text{CrSi}_n^-$  ( $n = 8-12$ ) with 355 nm photons. They speculated that the onset of endohedral structure may occur at  $n = 8$  but it is subject to further experimental and theoretical confirmation.

In order to explore the structural evolution of  $\text{CrSi}_n$  clusters, here we investigated  $\text{CrSi}_n^-$  ( $n = 3-12$ ) clusters using anion photoelectron spectroscopy and density functional theory calculations. Our study shows that the onset of endohedral structure for  $\text{CrSi}_n^-$  clusters actually occurs at  $n = 10$ . In addition, we found that the change of magnetic moments of  $\text{CrSi}_n^-$  clusters is related to their structural evolution.

## II. EXPERIMENTAL AND THEORETICAL METHODS

### A. Experimental

The experiments were conducted on a home-built apparatus consisting of a linear time-of-flight mass spectrometer (TOF-MS) and a magnetic-bottle photoelectron spectrometer, which has been described in details previously.<sup>16</sup> Briefly, the  $\text{CrSi}_n^-$  clusters were produced in a laser vaporization source by ablating a rotating translating disk target (13 mm diameter, Cr/Si mole ratio 1:4) with the second harmonic (532 nm) light pulses of a Nd:YAG laser (Continuum Surelite II-10). Helium carrier gas with  $\sim 4$  atm backing pressure was injected into the source by a pulsed valve to cool the formed clusters. The cluster anions were mass-analyzed by the time-of-flight mass spectrometer. The cluster anions of interest were mass-selected and decelerated before entering the photodetachment region. The photodetachment of the  $\text{CrSi}_n^-$  ( $n = 3-12$ ) clusters were conducted with the fourth harmonic light of a second Nd:YAG laser (Continuum Surelite II-10, 266 nm, 0.1–0.2 mJ/pulse). The photoelectrons were energy-analyzed by the magnetic-bottle photoelectron spectrometer. The electron binding energies were obtained by the energy-conserving relationship,  $\text{EBE} = h\nu - \text{EKE}$ , where  $h\nu$  is the photon energy used for photodetachment, EKE is the measured electron kinetic energy, and EBE is the electron binding energy. In this work, the photoelectron spectra were calibrated by the known

<sup>a)</sup> Author to whom correspondence should be addressed. Electronic mail: zhengwj@iccas.ac.cn. Tel: +86 10 62635054. Fax: +86 10 62563167.

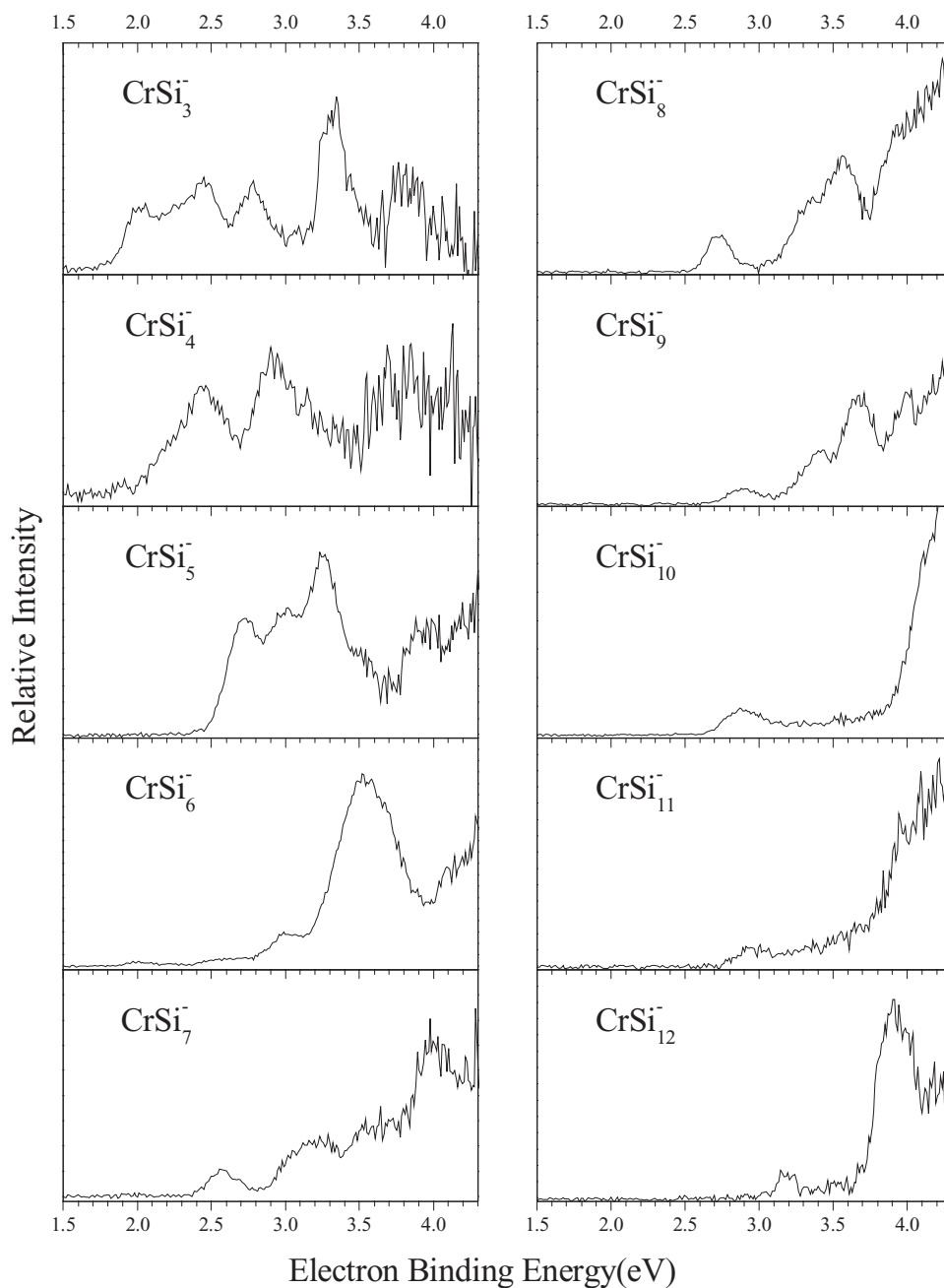


FIG. 1. Photoelectron spectra of  $\text{CrSi}_n^-$  ( $n = 3-12$ ) clusters obtained with 266 nm photons.

spectra of  $\text{Cu}^-$  and  $\text{I}^-$ . The energy resolution of the photoelectron spectrometer was  $\sim 40$  meV at the electron kinetic energy of 1 eV.

## B. Theoretical

The geometry optimization and frequency calculations of  $\text{CrSi}_n^-$  clusters were carried out employing the B3LYP functional theory<sup>58,59</sup> implemented in the Gaussian 09 program package.<sup>60</sup> The 6-311+g(d) basis set was used for both Cr and Si atoms. All the geometry optimizations were performed without any symmetry constraint. Many spin-multiplicities were considered during the calculations as a Cr atom has six unpaired electrons ( $3d^5 4s^1$ ). Harmonic vibrational frequencies were calculated to make sure that the structures corre-

spond to real local minima. The calculated total energies were corrected by the zero-point vibrational energies. The vertical detachment energies (VDEs) were calculated as the energy differences between the anion and neutral clusters at the same structures as those of the anions. The adiabatic detachment energies (ADEs) were obtained as the energy differences between the cluster anions and the optimized neutral clusters using the anion structures as initial structures.

## III. EXPERIMENTAL RESULTS

The photoelectron spectra of  $\text{CrSi}_n^-$  ( $n = 3-12$ ) clusters recorded with 266 nm photons are presented in Figure 1. The vertical detachment energies (VDEs) and the adiabatic detachment energies (ADEs) of  $\text{CrSi}_n^-$  ( $n = 3-12$ )

TABLE I. Experimental VDEs and ADEs estimated from the photoelectron spectra of  $\text{CrSi}_n^-$  ( $n = 3-12$ ).

Cluster	ADE (eV) <sup>a</sup>	VDE (eV) <sup>a</sup>	VDE (eV) <sup>b</sup>
$\text{CrSi}_3^-$	1.88(8) <sup>c</sup>	2.01(8)	–
$\text{CrSi}_4^-$	2.03(8)	2.45(8)	–
$\text{CrSi}_5^-$	2.52(8)	2.73(8)	–
$\text{CrSi}_6^-$	3.12(8)	3.53(8)	–
$\text{CrSi}_7^-$	2.42(8)	2.56(8)	–
$\text{CrSi}_8^-$	2.61(8)	2.72(8)	2.71(5)
$\text{CrSi}_9^-$	2.71(8)	2.90(8)	2.88(5)
$\text{CrSi}_{10}^-$	2.68(8)	2.88(8)	2.87(5)
$\text{CrSi}_{11}^-$	2.79(8)	2.97(8)	2.95(5)
$\text{CrSi}_{12}^-$	3.11(8)	3.19(8)	3.18(5)

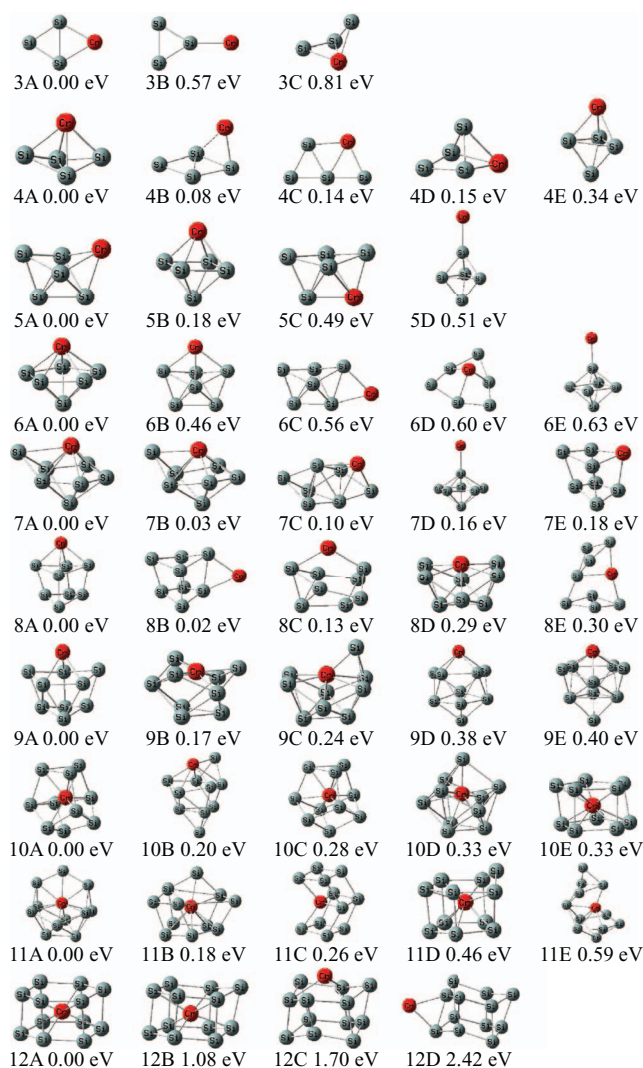
<sup>a</sup>This work.<sup>b</sup>Reference 6.<sup>c</sup>The numbers in parentheses indicate the uncertainties in the last digit.

clusters estimated from their photoelectron spectra are listed in Table I. The ADE from each spectrum was determined by drawing a straight line along the leading edge of the first peak to cross the baseline of the spectrum and adding the instrumental resolution to the EBE value at the crossing point. The VDEs were estimated from the maxima of the first peaks. The experimental VDEs of  $\text{CrSi}_n^-$  ( $n = 8-12$ ) have been measured by Bowen and co-workers previously.<sup>6</sup> As seen in Table I, the VDEs of  $\text{CrSi}_{8-12}^-$  measured in this work are in good agreement with their previous measurements.

As shown in Figure 1, the photoelectron spectrum of  $\text{CrSi}_3^-$  reveals five peaks centered at 2.01, 2.45, 2.78, 3.31, and 3.82 eV, respectively. In the spectrum of  $\text{CrSi}_4^-$ , there are two major peaks centered at 2.45 and 2.91 eV and a broad unresolved feature in the range of 3.50–4.20 eV. For  $\text{CrSi}_5^-$ , two major features are observed. The first one is in the range of 2.5–3.7 eV, and the second one in the range of 3.7–4.3 eV. The first feature is consisting of three peaks centered at 2.73, 2.99, and 3.26 eV and a shoulder at 3.50 eV. The second feature shows two barely discernible peaks centered at 3.9 and 4.2 eV. The spectrum of  $\text{CrSi}_6^-$  shows a strong broad feature centered at 3.53 eV. Some very weak low-binding energy features are also discernible at 2.0, 2.6, and 3.0 eV. These weak low EBE features are probably due to the existence of low-lying isomers in the experiment.

The spectrum of  $\text{CrSi}_7^-$  has four features centered at 2.56, 3.17, 3.64, and 3.98 eV, respectively.  $\text{CrSi}_8^-$  has three peaks centered at 2.72, 3.35, and 3.56, and a broad feature above 3.8 eV. Similar to  $\text{CrSi}_8^-$ ,  $\text{CrSi}_9^-$  has three peaks centered at 2.90, 3.43, and 3.67 eV, and a broad feature above 3.8 eV. The spectral shapes of  $\text{CrSi}_8^-$  and  $\text{CrSi}_9^-$  are quite similar although the VDE of  $\text{CrSi}_9^-$  shifts slightly toward higher electron binding energy compared to that of  $\text{CrSi}_8^-$ .

There is a significant change in the spectra of  $\text{CrSi}_n^-$  at  $n = 10$ . The spectra of  $\text{CrSi}_{10}^-$ ,  $\text{CrSi}_{11}^-$ , and  $\text{CrSi}_{12}^-$  are similar to each other but quite different from those of smaller  $\text{CrSi}_n^-$  clusters. The spectrum of  $\text{CrSi}_{10}^-$  has a weak low binding feature centered at 2.88 eV and a strong high binding feature over 3.9 eV. That of  $\text{CrSi}_{11}^-$  has a weak low binding feature centered at 2.97 eV and a strong high binding feature over 3.8 eV.  $\text{CrSi}_{12}^-$  has a weak low binding feature cen-

FIG. 2. Low-lying isomers of  $\text{CrSi}_n^-$  ( $n = 3-12$ ) clusters. The relative energies to the most stable isomers are shown under the geometric structures.

tered at 3.19 eV and a strong high binding feature over 3.7 eV (centered at  $\sim 3.90$  eV).  $\text{CrSi}_{10}^-$  has a HOMO–LUMO gap of at least 1.2 eV. The HOMO–LUMO gaps of  $\text{CrSi}_{11}^-$  and  $\text{CrSi}_{12}^-$  are  $\sim 1.0$  and  $\sim 0.7$  eV respectively, smaller than that of  $\text{CrSi}_{10}^-$ .

#### IV. THEORETICAL RESULTS

The structures of the low-lying isomers of  $\text{CrSi}_n^-$  ( $n = 3-12$ ) clusters from density functional theory calculations are displayed in Figure 2 with the most stable ones on the left. Their relative energies, theoretical VDEs and ADEs are listed in Table II along with the experimental VDEs and ADEs for comparison. The cartesian coordinates of the stable isomers of  $\text{CrSi}_n^-$  ( $n = 3-12$ ) clusters are available in the supplementary material.<sup>61</sup> We have also simulated the photoelectron spectra of different isomers based on theoretically generalized Koopman theorem (GKT)<sup>62,63</sup> and compared the simulated spectra with the experimental results in Figure 3. For convenient, we call the simulated spectra as density of states (DOS) spectra.<sup>63</sup> In the simulated DOS spectra, the peak of each transition

TABLE II. Relative energies of the calculated low-lying isomers of  $\text{CrSi}_n^-$  ( $n = 3-12$ ) as well as the comparison of their theoretical ADEs and VDEs to the experimental values. The isomers labeled in bold are the most probable isomers in the experiment.

Isomer	Sym.	State	$\Delta E$ (eV)	VDE (eV)		ADE (eV)		Isomer	Sym.	State	$\Delta E$ (eV)	VDE (eV)		ADE (eV)			
				Theo.	Expt.	Theo.	Expt.					Theo.	Expt.				
$\text{CrSi}_3^-$	<b>3A</b>	$C_{2v}$	${}^6A_1$	0.00	2.33	2.01	2.24	1.88	$\text{CrSi}_9^-$	<b>9A</b>	$C_1$	${}^6A$	0.00	2.76	2.90	2.63	2.71
	3B	$C_{2v}$	${}^6A_1$	0.57	2.05		1.44			<b>9B</b>	$C_{3v}$	${}^2A_1$	0.17	3.05		2.95	
	3C	$C_1$	${}^4A$	0.81	1.96		1.66			9C	$C_1$	${}^2A$	0.24	3.09		2.93	
$\text{CrSi}_4^-$	<b>4A</b>	$C_{2v}$	${}^4A_2$	0.00	2.16	2.45	1.93	2.03	9D	$C_s$	${}^6A'$	0.38	3.11		2.99		
	4B	$C_1$	${}^6A$	0.08	2.14		2.07		9E	$C_s$	${}^4A'$	0.40	2.85		2.58		
	4C	$C_s$	${}^4A''$	0.14	2.25		2.18		$\text{CrSi}_{10}^-$	<b>10A</b>	$C_1$	${}^2A$	0.00	3.23	2.88	2.92	2.68
	4D	$C_s$	${}^6A'$	0.15	2.25		1.94			10B	$C_s$	${}^6A'$	0.20	2.92		2.74	
	4E	$C_{3v}$	${}^4A_1$	0.34	2.69		2.38			10C	$C_1$	${}^4A$	0.28	3.51		3.24	
$\text{CrSi}_5^-$	<b>5A</b>	$C_s$	${}^6A'$	0.00	2.72	2.73	2.49	2.52	10D	$C_1$	${}^2A$	0.33	2.67		2.61		
	5B	$C_{4v}$	${}^4A_2$	0.18	2.66		2.22		10E	$C_1$	${}^2A$	0.33	3.27		3.14		
	5C	$C_s$	${}^4A''$	0.49	2.29		2.17		$\text{CrSi}_{11}^-$	<b>11A</b>	$C_1$	${}^2A$	0.00	3.17	2.97	3.03	2.79
	5D	$C_{3v}$	${}^6A_1$	0.51	2.81		2.60			11B	$C_1$	${}^2A$	0.18	3.38		3.23	
	$\text{CrSi}_6^-$	<b>6A</b>	$C_{5v}$	${}^4A_1$	0.00	3.19	3.53	3.00		3.12	<b>11C</b>	$C_2$	${}^2A$	0.26	3.13		2.93
<b>6B</b>		$C_{2v}$	${}^6A_1$	0.46	2.00		1.90		11D	$C_s$	${}^4A''$	0.46	3.31		2.73		
6C		$C_s$	${}^6A'$	0.56	2.15		2.04		11E	$C_1$	${}^2A$	0.59	3.47		3.29		
6D		$C_{3v}$	${}^6A$	0.60	2.95		2.90		$\text{CrSi}_{12}^-$	<b>12A</b>	$D_{3d}$	${}^2A_{1g}$	0.00	3.25	3.19	3.24	3.11
6E		$C_{4v}$	${}^6A_2$	0.63	2.83		2.38			12B	$C_1$	${}^4A$	1.08	2.81		2.41	
$\text{CrSi}_7^-$	<b>7A</b>	$C_s$	${}^6A'$	0.00	2.78	2.56	2.64	2.42		12C	$C_1$	${}^6A$	1.70	3.62		3.15	
	<b>7B</b>	$C_s$	${}^4A'$	0.03	2.67		2.42		12D	$C_s$	${}^6A'$	2.42	3.17		3.08		
	<b>7C</b>	$C_1$	${}^6A$	0.10	2.40		2.26										
	7D	$C_{5v}$	${}^6A_1$	0.16	2.63		2.33										
	7E	$C_1$	${}^4A$	0.18	2.61		2.37										
$\text{CrSi}_8^-$	<b>8A</b>	$C_{2v}$	${}^6A_1$	0.00	2.78	2.72	2.64	2.61									
	<b>8B</b>	$C_s$	${}^6A'$	0.02	3.04		2.82										
	<b>8C</b>	$C_s$	${}^6A'$	0.13	2.72		2.49										
	8D	$C_{2v}$	${}^2B_2$	0.29	3.17		3.06										
	8E	$C_s$	${}^4A''$	0.30	3.02		2.92										

corresponds to the removal of an electron from a specific molecular orbital of the cluster anion. During the simulation, the relative energies of the orbitals ( $\Delta E_n$ ) were calculated by the equation:  $\Delta E_n = E_{(\text{HOMO}-n)} - E_{\text{HOMO}}$ , where  $E_{(\text{HOMO}-n)}$  is the energy of the (HOMO-n) orbital from theoretical calculations,  $E_{\text{HOMO}}$  is the energy of the HOMO, and  $\Delta E_n$  is the relative energies of the (HOMO-n) orbital compared to the HOMO. Then, the first peak associated with the HOMO was set at the position of VDE, and the peaks associated with the deeper orbitals were shifted to higher binding energies according to the values of  $-\Delta E_n$ . The peak associated with each orbital was fitted with a unit-area Gaussian function of 0.2 eV full width at half maximum.

### A. $\text{CrSi}_3^-$

As shown in Figure 2, our calculations found three low-lying isomers for  $\text{CrSi}_3^-$ . Isomer 3A can be described as the Cr atom substituting one of the Si atoms in the  $\text{Si}_4$  rhombus. Isomer 3B has the Cr atom attaching to a corner of the  $\text{Si}_3$  triangle. Isomer 3C is a tetrahedral structure. The calculated VDEs of isomer 3A, 3B, and 3C are 2.33, 2.05, and 1.96 eV, respectively. They can be considered as in reasonable agreement with the experimental VDE (2.01 eV) at this level of theory. The theoretical VDEs of isomers 3B and 3C are closer to the experimental value than that of isomer 3A. However, iso-

mers 3B and 3C are 0.57 eV and 0.81 eV higher in energy than isomer 3A, much less stable than isomer 3A. It is unlikely for isomers 3B and 3C to exist in the experiment. In Figure 3, we can see that the simulated DOS spectrum of isomer 3A is more similar to the experimental spectrum than those of isomers 3B and 3C. Therefore, the experimental spectrum of  $\text{CrSi}_3^-$  is more likely contributed by isomer 3A. In addition, the structure of isomer 3A is consistent with the neutral  $\text{CrSi}_3$  structure calculated by Han and Hagelberg.<sup>38</sup>

### B. $\text{CrSi}_4^-$

Our calculations show that the most stable structure of  $\text{CrSi}_4^-$  cluster (4A) is a  $C_{2v}$  trigonal bipyramidal structure. In the structure of isomer 4B, the chromium atom connects to the vertex of the  $\text{Si}_4$  rhombus out of plane. The structure of isomer 4C is a quasi-plane trapezium with the Cr atom slightly off the plane. Isomer 4D can be seen as the Cr atom and three silicon atoms form a distorted rhombus and have the fourth silicon atom staying above them. The structure of isomer 4E is a  $C_{3v}$  symmetry trigonal bipyramidal structure. Isomers 4B, 4C, 4D, and 4E are higher in energy than isomer 4A by 0.08, 0.14, 0.15, and 0.34 eV. The calculated VDEs of isomer 4A, 4B, 4C, 4D, and 4E are 2.16, 2.14, 2.25, 2.25, and 2.69 eV, respectively, all in reasonable agreement with the experimental measurement (2.45 eV). Although the VDEs of isomer 4C

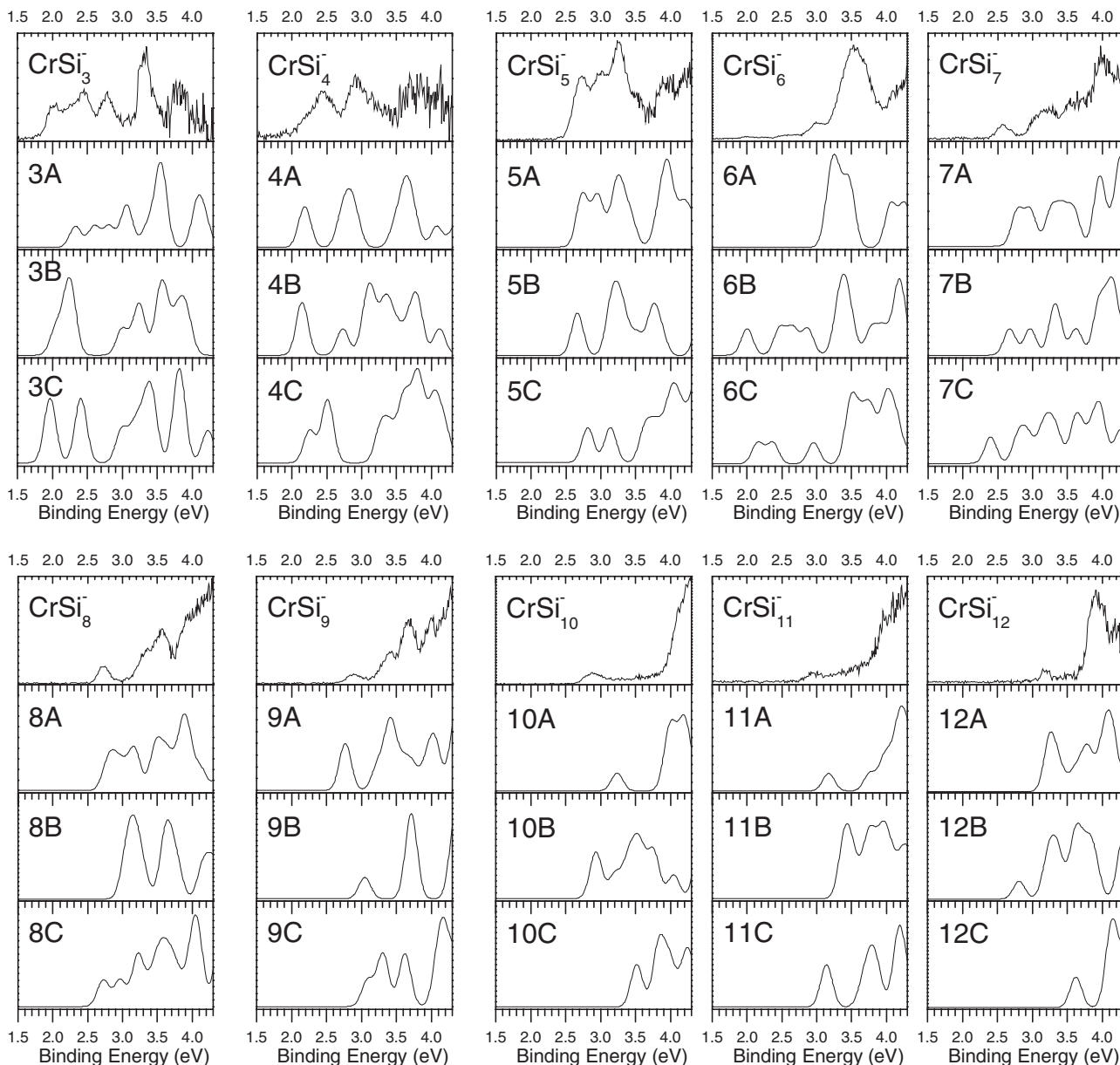


FIG. 3. Comparison of the experimental photoelectron spectra of  $\text{CrSi}_n^-$  ( $n=3-12$ ) clusters with their simulated DOS spectra. The simulations were conducted by fitting the distribution of the transition lines with unit-area Gaussian functions of 0.2 eV full width at half maximum.

and 4D are closer to the experimental value than isomer 4A, the simulated DOS spectrum of isomer 4A agrees with the experimental spectrum better. Therefore, we suggest isomer 4A to be the most probable one observed in the experiment.

### C. $\text{CrSi}_5^-$

For  $\text{CrSi}_5^-$ , isomers 5A and 5C are formed by substituting one of the Si atoms in the  $\text{Si}_6$  compact structure with a Cr atom. The original  $\text{Si}_6$  structure is changed slightly due to the Cr substitution. It seems the Cr atom prefers to substitute a low-coordination site since isomer 5C is less stable than isomer 5A by 0.49 eV. Isomer 5B is a  $C_{4v}$  tetragonal bipyramid. It is higher than isomer 5A by 0.18 eV in energy. Isomer 5D has  $C_{3v}$  symmetry and can be viewed as the Cr atom attaching to the vertex of a  $\text{Si}_5$  trigonal bipyramid. Isomer 5D is

higher in energy than isomer 5A by 0.51 eV. The theoretical VDE (2.72 eV) of isomer 5A is very close to the experimental VDE (2.73 eV). The simulated DOS spectrum of isomer 5A is also consistent with the experimental spectrum. We suggest isomer 5A to be the most probable structure for  $\text{CrSi}_5^-$ .

### D. $\text{CrSi}_6^-$

The most stable isomer of  $\text{CrSi}_6^-$  (6A) is a  $C_{5v}$  symmetry pentagonal bipyramidal structure with the Cr atom occupying a vertex site. Isomers 6B and 6C are formed by adding the Cr atom to different sites of the  $\text{Si}_6$  compact structure composed of three tetrahedrons. Isomer 6D has a  $C_{3v}$  symmetry structure with the Cr atom sitting right above a bowl formed by six silicon atoms. In isomer 6E, the Cr atom attaches to a vertex of the  $\text{Si}_6$  tetragonal bipyramid. Isomers 6B, 6C, 6D, and 6E are

higher in energy than isomer 6A by 0.46, 0.56, 0.60, and 0.63 eV, respectively. The calculated VDE of isomer 6A is  $\sim 3.19$  eV. The VDEs of isomers 6B, 6C, 6D, and 6E are calculated to be 2.00, 2.15, 2.95, and 2.83 eV. The structures of  $\text{CrSi}_6^-$  found by our calculations are different from the  $O_h$  symmetry endohedral structure of neutral  $\text{CrSi}_6$  reported by Han and Hagelberg.<sup>38</sup> Based on the simulated DOS spectra in Figure 3, the 3.53 eV major peak in the experimental photoelectron spectrum of  $\text{CrSi}_6^-$  is more likely contributed by isomer 6A. The weak features at 2.0, 2.6, and 3.0 eV in the experimental spectrum of  $\text{CrSi}_6^-$  probably are contributed by isomer 6B as its simulated DOS spectrum has peaks at the positions of these weak features.

The weak low EBE features observed in the experimental photoelectron spectrum of  $\text{CrSi}_6^-$  are similar to the low EBE features in the spectrum of  $\text{TbSi}_6^-$  measured by Ohara *et al.*,<sup>64</sup> the spectrum of  $\text{HoSi}_6^-$ ,  $\text{GdSi}_6^-$ , and  $\text{PrSi}_6^-$  measured by Grubisic *et al.*,<sup>13</sup> and that of  $\text{ScSi}_6^-$  measured by Xu *et al.*<sup>17</sup> Xu *et al.* suggested that those weak low EBE features are due to the existence of the less stable isomers. Our results on  $\text{CrSi}_6^-$  cluster are in agreement with their work.

### E. $\text{CrSi}_7^-$

The first two isomers (7A and 7B) of  $\text{CrSi}_7^-$  are nearly degenerate in energy, with isomer 7B higher than isomer 7A by only 0.03 eV. Both isomers 7A and 7B can be considered as evolved from isomer 6A by attaching a silicon atom to the pentagonal bipyramid. They have similar geometric structures but different spin multiplicities. Isomer 7A is at  $^6A'$  state whereas isomer 7B belongs to  $^4A'$  state. The structure of isomer 7C can be viewed as the Cr atom substitutes one of the silicon atoms in the  $\text{Si}_8$  compact structure. Isomer 7D has  $C_{5v}$  symmetry with the Cr atom attaching to a vertex of the  $\text{Si}_7$  pentagonal bipyramid. In isomer 7E, the Cr atom and the seven silicon atoms form a distorted tetragonal prism. Isomers 7C, 7D, and 7E are higher in energy than isomer 7A by 0.10, 0.16, and 0.18 eV, respectively. The theoretical VDEs of isomer 7A, 7B, 7C, 7D, and 7E are 2.78, 2.67, 2.40, 2.63, and 2.61 eV, respectively. The simulated DOS spectrum of isomer 7A is similar to the experimental spectrum. Hence, isomer 7A might be the most probable one detected in the experiment. Isomers 7B and 7C may also exist in the experiment since their total energies are very close to that of isomer 7A and their VDEs are close to experimental value as well.

### F. $\text{CrSi}_8^-$

Similar to  $\text{CrSi}_7^-$ , the first two isomers of  $\text{CrSi}_8^-$  are also degenerate in energy. Isomer 8B is higher than isomer 8A by only 0.02 eV. In isomer 8A, the Cr atom capes one face of the distorted tetragonal prism formed by  $\text{Si}_8$ . While in isomer 8B, the Cr atom attaches to one edge of the distorted tetragonal prism. The structure of isomer 8C can be described as a Cr atom interacts with the two ends of the  $\text{Si}_8$  boat structure. Isomer 8D has  $C_{2v}$  symmetry with the Cr atom interacting with a  $\text{Si}_8$  basin structure, which is similar to the bowl shape of  $\text{Si}_8\text{Cr}$  structure reported by Kawamura *et al.*<sup>57</sup> In iso-

mer 8E, the Cr atom is surrounded by two tilting distorted  $\text{Si}_4$  rhombuses. Isomer 8C, 8D, and 8E are higher in energy than isomer 8A by 0.13, 0.29, and 0.30 eV, respectively. The theoretical VDEs of 8A, 8B, 8C, 8D, and 8E are 2.78, 3.04, 2.72, 3.17, and 3.02 eV, respectively. The VDEs of isomers 8A and 8C are very close to the experimental VDE (2.72 eV), while that of isomer 8B is slightly higher than the experimental VDE. Since isomers 8A, 8B, and 8C are very close in energy, it might be possible that they are all stable enough to exist in our experiments. The simulated DOS spectra of isomers 8A and 8C show most of the features in the experimental spectrum. Therefore, we suggest that isomers 8A and 8C both contribute to the observed spectrum of  $\text{CrSi}_8^-$ . The simulated DOS spectrum of isomer 8B is very different from the experimental spectrum, but its existence cannot be ruled out. It may contribute to some of the higher EBE features in the experimental spectrum.

### G. $\text{CrSi}_9^-$

The most stable structure of  $\text{CrSi}_9^-$ , isomer 9A, is in  $^6A$  state. It can be considered as a distorted  $\text{Si}_4$  rhombus and a  $\text{Si}_5$  five-membered ring stacking together then having the Cr atom sitting right above the  $\text{Si}_5$  five-membered ring. Isomer 9B has a  $C_{3v}$  structure with the Cr atom surrounded by a chair-style  $\text{Si}_6$  ring and then adding a  $\text{Si}_3$  to the bottom. Isomer 9C is derived from isomer 8D by adding a Si atom to the edge of the  $\text{Si}_8$  basin. Isomer 9D is combined by a  $\text{Si}_5$  tetragonal pyramid and a  $\text{CrSi}_4$  tetragonal pyramid. Isomer 9E is combined by a  $\text{Si}_4$  trigonal pyramid and a distorted  $\text{CrSi}_5$  pentagonal pyramid. Isomers 9B, 9C, 9D, and 9E are higher in energy than isomer 9A by 0.17, 0.24, 0.38, and 0.40 eV, respectively. The calculated VDEs of isomer 9A, 9B, 9C, 9D, and 9E are 2.76, 3.05, 3.09, 3.11, and 2.85 eV, respectively, all close to the experimental VDE of 2.90 eV. According to the simulated DOS spectra in Figure 3, isomers 9A and 9B may coexist in the experiment.

### H. $\text{CrSi}_{10}^-$

The most stable structure of  $\text{CrSi}_{10}^-$  (isomer 10A) is an endohedral structure with the Cr atom encapsulated in a  $\text{Si}_{10}$  silicon cage. The  $\text{Si}_{10}$  silicon cage is formed by a triangle on the top, three five-membered rings in the middle, and three distorted rhombuses at the bottom. Isomer 10B has an exohedral structure. Isomers 10C, 10D, and 10E all have endohedral structures. It is worth mentioning that, in isomer 10E, the Cr atom is sandwiched by two  $\text{Si}_5$  rings. Isomer 10B, 10C, 10D, and 10E are 0.20, 0.28, 0.33, and 0.33 eV higher in energy than isomer 10A. The calculated VDEs of isomer 10A, 10B, 10C, 10D, and 10E are 3.23, 2.92, 3.51, 2.67, and 3.27 eV, respectively. The VDEs of isomers 10A and 10B are in reasonable agreement with the experimental value (2.88 eV). Although the VDE of isomer 10B is closer to the experimental value than that of isomer 10A, its simulated DOS spectrum is less similar to the experimental spectrum of  $\text{CrSi}_{10}^-$  than that of isomer 10A. Hence, we suggest isomer 10A to be the most probable structure for  $\text{CrSi}_{10}^-$  cluster.

### I. $\text{CrSi}_{11}^-$

The most stable structure of  $\text{CrSi}_{11}^-$ , isomer 11A, has  $^2A$  state endohedral structure with the Cr atom sitting in the center of a basket-shaped silicon cage formed by eleven Si atoms. It can be considered as derived from isomer 8D by adding three silicon atoms as the basket handle. Isomer 11B has the Cr atom sandwiched by two  $\text{Si}_5$  rings and has an additional Si atom connecting to the Cr atom and one edge of the upper  $\text{Si}_5$  ring. The upper  $\text{Si}_5$  ring is relative loose with very large Si-Si distances. Isomer 11C can be seen as two distorted tetragonal prisms stacking together with the Cr atom in the middle. In isomer 11D, the Cr atom is sandwiched by a  $\text{Si}_5$  ring and a distorted  $\text{Si}_6$  ring. Isomer 11E is evolved from isomer 7A by adding a  $\text{Si}_4$  tetrahedron on the top. Isomers 11B, 11C, 11D, and 11E are higher in energy than isomer 11A by 0.18, 0.26, 0.46, and 0.59 eV, respectively. The calculated VDEs of 11A–11E are 3.17, 3.38, 3.13, 3.31, and 3.47 eV, respectively. The VDEs of isomer 11A and 11C are close to our observed data of  $\text{CrSi}_{11}^-$  cluster (2.97 eV), they may contribute to the experimental photoelectron spectra. The simulated DOS spectrum of isomer 11A agrees well with the experimental spectrum. That indicates that isomer 11A probably is the major species in our experiment. The structure of isomer 11A for  $\text{CrSi}_{11}^-$  cluster is in agreement with the theoretical calculations of neutral  $\text{CrSi}_{11}$  by Khanna *et al.*<sup>23</sup>

### J. $\text{CrSi}_{12}^-$

Our calculations show that the most stable structure of  $\text{CrSi}_{12}^-$ , isomer 12A, is in  $^2A$  state and  $D_{3d}$  symmetry with the Cr atom being encapsulated in a  $\text{Si}_{12}$  hexagonal prism cage. Isomer 12B is in  $^4A$  state. The structure of isomer 12B is similar to that of isomer 12A with a little distortion in the  $\text{Si}_{12}$  hexagonal prism cage, which lowers its symmetry to  $C_1$ . Isomers 12C and 12D have exohedral structures with the Cr atom capping the top or attaching to the edge of the distorted silicon cage. Isomer 12B, 12C, and 12D are higher in energy than isomer 12A by 1.08, 1.70, and 2.42 eV, respectively, much less stable than isomer 12A. This implies that isomers 12B, 12C and 12D probably do not exist in our experiment. The calculated VDE of isomer 12A is about 3.25 eV, in good agreement with the experimental value of 3.19 eV. The theoretical calculations of Khanna *et al.*<sup>23</sup> show that neutral  $\text{CrSi}_{12}$  cluster has  $D_{6h}$  geometry with the Cr atom sandwiched by two  $\text{Si}_6$  regular hexagons. Isomer 12A of  $\text{CrSi}_{12}^-$  from our calculations are basically in agreement with that reported by Khanna *et al.*, although the structure of  $\text{CrSi}_{12}^-$  cluster found in this work is slightly distorted to  $D_{3d}$  structure. The difference is probably due to the additional of the excess electron or the different theoretical methods used in our calculations.

## V. DISCUSSION

From Figure 2, we can see that the most stable isomers of  $\text{CrSi}_n^-$  ( $n = 3-9$ ) are all exohedral structures while those of  $\text{CrSi}_{10}^-$ ,  $\text{CrSi}_{11}^-$ , and  $\text{CrSi}_{12}^-$  are endohedral structures. This is in agreement with the change in the experimental photoelectron spectra observed in Figure 1. It is also consistent

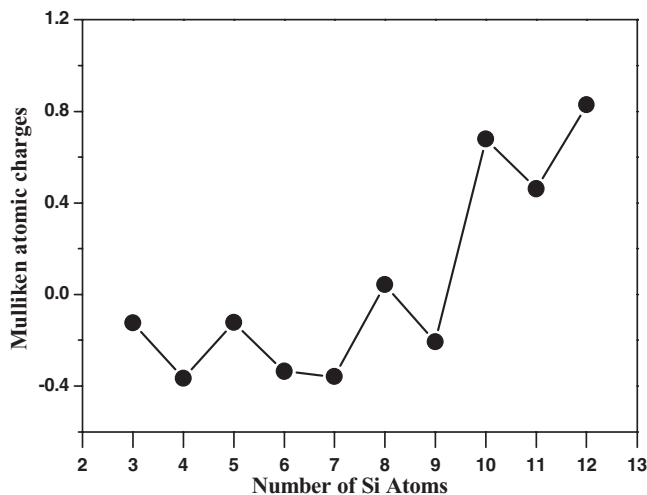


FIG. 4. Mulliken atomic charges on Cr atom for  $\text{CrSi}_n^-$  ( $n = 3-12$ ) clusters.

with the argon physisorption experiments of  $\text{CrSi}_n^+$  cations conducted by Janssens *et al.* who found the argon physisorption on  $\text{CrSi}_n^+$  drops at  $n = 10$ .<sup>14</sup> The onset of endohedral structure at  $n = 10$  for  $\text{CrSi}_n^-$  clusters is different from the case of  $\text{CuSi}_n^-$ , in which the endohedral structures show up at  $n = 12$ .<sup>19</sup> It is worth mentioning that the structures of  $\text{CrSi}_{10}^-$ ,  $\text{CrSi}_{11}^-$ , and  $\text{CrSi}_{12}^-$  from our calculations are basically similar to those found by Kawamura *et al.*<sup>57</sup> Although Kawamura *et al.* defined the structures of  $\text{CrSi}_{8-11}$  clusters as incomplete encapsulation and that of  $\text{CrSi}_{12}$  as complete encapsulation, our experimental results imply that  $\text{CrSi}_{10}^-$ ,  $\text{CrSi}_{11}^-$ , and  $\text{CrSi}_{12}^-$  belong to the same category according to the similarities in their photoelectron spectra. Interestingly, it seems the change of magnetic properties of the  $\text{CrSi}_n^-$  clusters is correlated to their geometric structures. As we can see in Table II, the most stable isomers of  $\text{CrSi}_n^-$  from  $n = 3$  to 9 have larger magnetic moments than the most stable isomers of  $\text{CrSi}_{10}^-$ ,  $\text{CrSi}_{11}^-$ , and  $\text{CrSi}_{12}^-$ . The most stable isomers of  $\text{CrSi}_n^-$  clusters with  $n = 3, 5, 7-9$  have magnetic moments of  $5\mu_B$  and those of  $\text{CrSi}_4^-$  and  $\text{CrSi}_6^-$  have magnetic moments of  $3\mu_B$ ; while the magnetic moments of  $\text{CrSi}_{10}^-$ ,  $\text{CrSi}_{11}^-$ , and  $\text{CrSi}_{12}^-$  are only  $1\mu_B$ . That indicates that the magnetic moment of Cr atom is quenched due to the encapsulation of Cr atom by silicon cage.

Figure 4 shows the Mulliken atomic charges on Cr atom for  $\text{CrSi}_n^-$  ( $n = 3-12$ ) clusters. It can be seen that the charges on the Cr atom are negative or near zero for  $\text{CrSi}_n^-$  clusters with  $n = 3-9$  and the positive charge on Cr atom increases significantly when  $n$  increases from 9 to 10. The charges on Cr atom are approximately +0.68 e, +0.46 e, and +0.83 e for  $\text{CrSi}_{10}^-$ ,  $\text{CrSi}_{11}^-$ , and  $\text{CrSi}_{12}^-$  clusters. The Mulliken atomic charges analysis indicates that the negative charge of  $\text{CrSi}_n^-$  clusters mainly localizes at the cluster surface. The Cr atom in  $\text{CrSi}_{10}^-$ ,  $\text{CrSi}_{11}^-$ , and  $\text{CrSi}_{12}^-$  is positive charged since it donates electron to the silicon atoms and it is encapsulated in the silicon cage. The charge distribution on Cr atom is also related to the evolution of the geometric structures of  $\text{CrSi}_n^-$  clusters.

Here, we compare the structures of  $\text{CrSi}_n^-$  clusters with those of  $\text{ScSi}_n^-$  ( $n = 2-6$ ) and  $\text{VSi}_n^-$  ( $n = 3-6$ ) clusters.<sup>16,17</sup>

The most stable structures of  $\text{ScSi}_6^-$ ,  $\text{VSi}_6^-$ , and  $\text{CrSi}_6^-$  are very similar, but there are some differences in the structures of  $\text{MSi}_{3-5}^-$  ( $M = \text{Sc}, \text{V}$  and  $\text{Cr}$ ). The most stable isomers of  $\text{ScSi}_3^-$  and  $\text{CrSi}_3^-$  are both planar rhombus while that of  $\text{VSi}_3^-$  is a tetrahedron. For  $\text{MSi}_4^-$ , the most stable isomers of  $\text{CrSi}_4^-$  and  $\text{VSi}_4^-$  are both  $C_{2v}$  structures with the  $M$  atom staying above a bend  $\text{Si}_4$  rhombus, while that of  $\text{ScSi}_4^-$  is a  $C_{3v}$  trigonal bipyramid. The most stable isomer of  $\text{CrSi}_5^-$  can be viewed as the  $\text{Cr}$  atom face-capping a  $\text{Si}_5$  trigonal bipyramid, that of  $\text{ScSi}_5^-$  is similar to isomer 5C of  $\text{CrSi}_5^-$ , while that of  $\text{VSi}_5^-$  is a  $C_{4v}$  tetragonal bipyramid similar to isomer 5B of  $\text{CrSi}_5^-$ .

In the  $\text{CrSi}_n^-$  ( $n = 3-6$ ) clusters, the Si-Si bond lengths are in the range of 2.30–2.61 Å, slightly shorter than the Cr-Si bond lengths (2.54–2.63 Å). Similarly, the Si-Si bond lengths (2.21–2.56 Å) in  $\text{ScSi}_n^-$  clusters are also shorter than the Sc-Si bond lengths (2.52–2.73 Å).<sup>17</sup> But it is not the case in  $\text{VSi}_n^-$  clusters, in which the Si-Si bond lengths (2.38–2.59 Å) are rather longer than the V-Si bond lengths (2.26–2.55 Å) in general.<sup>16</sup> It seems that the Cr-Si interactions are slightly stronger than the Sc-Si interactions but weaker than the V-Si interactions. On the other hand, the Si-Si interactions in  $\text{CrSi}_n^-$  clusters are slightly weaker than those in  $\text{ScSi}_n^-$  but stronger than those in  $\text{VSi}_n^-$ . Based on these, it can be suggested that strong M-Si interactions may weaken the Si-Si interactions in silicon clusters.

## VI. CONCLUSIONS

We investigated  $\text{CrSi}_n^-$  ( $n = 3-12$ ) clusters with anion photoelectron spectroscopy and density functional theory calculations. The combination of experimental measurements and theoretical calculations shows that the emerging of endohedral structure for  $\text{CrSi}_n^-$  clusters starts at  $n = 10$ . The most stable structure of  $\text{CrSi}_{10}^-$  is an endohedral structure with the Cr atom encapsulated in a  $\text{Si}_{10}$  silicon cage composed of a triangle, three five-membered rings, and three rhombuses. That of  $\text{CrSi}_{11}^-$  is an endohedral structure with the Cr atom sitting at the center of a basket-shaped silicon cage formed by eleven Si atoms.  $\text{CrSi}_{12}^-$  has a  $D_{3d}$  structure with the Cr atom encapsulated in a  $\text{Si}_{12}$  hexagonal prism cage. The magnetic properties of the  $\text{CrSi}_n^-$  clusters are correlated to their geometric structures. The most stable isomers of  $\text{CrSi}_n^-$  for  $n = 3-9$  have exohedral structures and their magnetic moments are in the range of 3–5 $\mu_B$ , while those of  $\text{CrSi}_{10}^-$ ,  $\text{CrSi}_{11}^-$ , and  $\text{CrSi}_{12}^-$  have endohedral structures and magnetic moments of 1 $\mu_B$ . The change of the charges on Cr atom is correlated to the evolution of the geometric structures of  $\text{CrSi}_n^-$  ( $n = 3-12$ ) clusters.

## ACKNOWLEDGMENTS

This work was supported by the Knowledge Innovation Program of the Chinese Academy of Sciences (Grant No. KJCX2-EW-H01) and the Natural Science Foundation of China (Grant No. 21103202). The theoretical calculations were conducted on the ScGrid and Deepcomp7000 of the Supercomputing Center, Computer Network Information Center of the Chinese Academy of Sciences.

- <sup>1</sup>N. A. Antonis, M. Giannis, E. F. George, and M. Madhu, *New J. Phys.* **4**, 78 (2002).
- <sup>2</sup>S. M. Beck, *J. Chem. Phys.* **87**, 4233 (1987).
- <sup>3</sup>S. M. Beck, *J. Chem. Phys.* **90**, 6306 (1989).
- <sup>4</sup>H. Hiura, T. Miyazaki, and T. Kanayama, *Phys. Rev. Lett.* **86**, 1733 (2001).
- <sup>5</sup>M. Ohara, K. Koyasu, A. Nakajima, and K. Kaya, *Chem. Phys. Lett.* **371**, 490 (2003).
- <sup>6</sup>W. J. Zheng, J. M. Nilles, D. Radisic, and J. K. H. Bowen, *J. Chem. Phys.* **122**, 071101 (2005).
- <sup>7</sup>K. Koyasu, M. Akutsu, M. Mitsui, and A. Nakajima, *J. Am. Chem. Soc.* **127**, 4998 (2005).
- <sup>8</sup>S. Neukermans, X. Wang, N. Veldeman, E. Janssens, R. E. Silverans, and P. Lievens, *Int. J. Mass Spectrom.* **252**, 145 (2006).
- <sup>9</sup>K. Koyasu, J. Atobe, S. Furuse, and A. Nakajima, *J. Chem. Phys.* **129**, 214301 (2008).
- <sup>10</sup>S. Furuse, K. Koyasu, J. Atobe, and A. Nakajima, *J. Chem. Phys.* **129**, 064311 (2008).
- <sup>11</sup>P. Gruene, A. Fielicke, G. Meijer, E. Janssens, V. T. Ngan, M. T. Nguyen, and P. Lievens, *ChemPhysChem* **9**, 703 (2008).
- <sup>12</sup>A. Grubisic, H. Wang, Y. J. Ko, and K. H. Bowen, *J. Chem. Phys.* **129**, 054302 (2008).
- <sup>13</sup>A. Grubisic, Y. J. Ko, H. Wang, and K. H. Bowen, *J. Am. Chem. Soc.* **131**, 10783 (2009).
- <sup>14</sup>E. Janssens, P. Gruene, G. Meijer, L. Woste, P. Lievens, and A. Fielicke, *Phys. Rev. Lett.* **99**, 063401 (2007).
- <sup>15</sup>J. T. Lau, K. Hirsch, P. Klar, A. Langenberg, F. Lofink, R. Richter, J. Rittmann, M. Vogel, V. Zamudio-Bayer, T. Möller, and B. v. Issendorff, *Phys. Rev. A* **79**, 053201 (2009).
- <sup>16</sup>H.-G. Xu, Z.-G. Zhang, Y. Feng, J. Y. Yuan, Y. C. Zhao, and W. J. Zheng, *Chem. Phys. Lett.* **487**, 204 (2010).
- <sup>17</sup>H. G. Xu, M. M. Wu, Z. G. Zhang, Q. Sun, and W. J. Zheng, *Chin. Phys. B* **20**, 043102 (2011).
- <sup>18</sup>H.-G. Xu, Z.-G. Zhang, Y. Feng, and W.-J. Zheng, *Chem. Phys. Lett.* **498**, 22 (2010).
- <sup>19</sup>H.-G. Xu, M. M. Wu, Z.-G. Zhang, J. Y. Yuan, Q. Sun, and W. J. Zheng, *J. Chem. Phys.* **136**, 104308 (2012).
- <sup>20</sup>R. Robles and S. N. Khanna, *Phys. Rev. B* **80**, 115414 (2009).
- <sup>21</sup>A. P. Yang, Z. Y. Ren, P. Guo, and G. H. Wang, *J. Mol. Struct.-THEOCHEM* **856**, 88 (2008).
- <sup>22</sup>V. Kumar and Y. Kawazoe, *Phys. Rev. Lett.* **87**, 045503 (2001).
- <sup>23</sup>S. N. Khanna, B. K. Rao, and P. Jena, *Phys. Rev. Lett.* **89**, 016803 (2002).
- <sup>24</sup>J. Lu and S. Nagase, *Phys. Rev. Lett.* **90**, 115506 (2003).
- <sup>25</sup>A. K. Singh, T. M. Briere, V. Kumar, and Y. Kawazoe, *Phys. Rev. Lett.* **91**, 146802 (2003).
- <sup>26</sup>G. Mpourmpakis, G. E. Froudakis, A. N. Andriotis, and M. Menon, *Phys. Rev. B* **68**, 125407 (2003).
- <sup>27</sup>G. Mpourmpakis, G. E. Froudakis, A. N. Andriotis, and M. Menon, *J. Chem. Phys.* **119**, 7498 (2003).
- <sup>28</sup>P. Guo, Z. Y. Ren, F. Wang, J. Bian, J. G. Han and G. H. Wang, *J. Chem. Phys.* **121**, 12265 (2004).
- <sup>29</sup>A. Negishi, N. Kariya, K. Sugawara, I. Arai, H. Hiura, and T. Kanayama, *Chem. Phys. Lett.* **388**, 463 (2004).
- <sup>30</sup>J. Wang and J. G. Han, *J. Chem. Phys.* **123**, 064306 (2005).
- <sup>31</sup>J. U. Reveles and S. N. Khanna, *Phys. Rev. B* **74**, 035435 (2006).
- <sup>32</sup>E. N. Koukaras, C. S. Garoufalidis, and A. D. Zdetsis, *Phys. Rev. B* **73**, 235417 (2006).
- <sup>33</sup>J. G. Han, R. N. Zhao, and Y. H. Duan, *J. Phys. Chem. A* **111**, 2148 (2007).
- <sup>34</sup>L. Z. Kong and J. R. Chelikowsky, *Phys. Rev. B* **77**, 073401 (2008).
- <sup>35</sup>R. Robles, S. N. Khanna, and A. W. Castleman, *Phys. Rev. B* **77**, 235441 (2008).
- <sup>36</sup>J. Wang and J. H. Liu, *J. Phys. Chem. A* **112**, 4562 (2008).
- <sup>37</sup>K. Jackson and B. Nellermoe, *Chem. Phys. Lett.* **254**, 249 (1996).
- <sup>38</sup>J.-G. Han and F. Hagelberg, *Chem. Phys.* **263**, 255 (2001).
- <sup>39</sup>J.-G. Han, C. Xiao, and F. Hagelberg, *Struct. Chem.* **13**, 173 (2002).
- <sup>40</sup>V. Kumar and Y. Kawazoe, *Phys. Rev. B* **65**, 073404 (2002).
- <sup>41</sup>R. Robles and S. N. Khanna, *J. Chem. Phys.* **130**, 164313 (2009).
- <sup>42</sup>R.-N. Zhao, J.-G. Han, J.-T. Bai, and L.-S. Sheng, *Chem. Phys.* **378**, 82 (2010).
- <sup>43</sup>G. Li, W. Ma, A. Gao, H. Chen, D. Finlow, and Q.-S. Li, *J. Theor. Comput. Chem.* **11**, 185 (2012).
- <sup>44</sup>Y. Liu, G. L. Li, A. M. Gao, H. Y. Chen, D. Finlow, and Q. S. Li, *Eur. Phys. J. D* **64**, 27 (2011).
- <sup>45</sup>R.-N. Zhao, J.-G. Han, J.-T. Bai, F.-Y. Liu, and L.-S. Sheng, *Chem. Phys.* **372**, 89 (2010).

- <sup>46</sup>J. Wang, Q.-M. Ma, R.-P. Xu, Y. Liu, and Y.-C. Li, *Phys. Lett. A* **373**, 2869 (2009).
- <sup>47</sup>J.-R. Li, G.-H. Wang, C.-H. Yao, Y.-W. Mu, J.-G. Wan, and M. Han, *J. Chem. Phys.* **130**, 164514 (2009).
- <sup>48</sup>J.-R. Li, C.-H. Yao, Y.-W. Mu, J.-G. Wan, and M. Han, *J. Mol. Struct.-THEOCHEM* **916**, 139 (2009).
- <sup>49</sup>J.-G. Han and F. Hagelberg, *J. Mol. Struct.-THEOCHEM* **549**, 165 (2001).
- <sup>50</sup>G.-F. Zhao, J.-M. Sun, Y.-Z. Gu, and Y.-X. Wang, *J. Chem. Phys.* **131**, 114312 (2009).
- <sup>51</sup>R. K. Waits, *Thin Solid Films* **16**, 237 (1973).
- <sup>52</sup>M. Jhabvala, R. S. Babu, C. Monroy, M. M. Freund, and C. D. Dowell, *Cryogenics* **42**, 517 (2002).
- <sup>53</sup>D. Caputo, G. de Cesare, A. Nascetti, and M. Tucci, *Thin Solid Films* **515**, 7517 (2007).
- <sup>54</sup>R. K. Waits, *Proc. IEEE* **59**, 1425 (1971).
- <sup>55</sup>M.-T. Chang, C.-Y. Chen, L.-J. Chou, and L.-J. Chen, *ACS Nano* **3**, 3776 (2009).
- <sup>56</sup>J. G. Han and Y. Y. Shi, *Chem. Phys.* **266**, 33 (2001).
- <sup>57</sup>H. Kawamura, V. Kumar, and Y. Kawazoe, *Phys. Rev. B* **70**, 245433 (2004).
- <sup>58</sup>A. Becke, *J. Chem. Phys.* **98**, 5648 (1993).
- <sup>59</sup>C. Lee, W. Yang, and R. G. Parr, *Phys. Rev. B* **37**, 785 (1988).
- <sup>60</sup>M. J. Frisch, G. W. Trucks, H. B. Schlegel, *et al.*, GAUSSIAN 09, Revision A.02, Gaussian, Inc. Wallingford CT, 2009.
- <sup>61</sup>See supplementary material at <http://dx.doi.org/10.1063/1.4742065> for the cartesian coordinates of the stable isomers of CrSi<sub>n</sub><sup>-</sup> clusters.
- <sup>62</sup>J. T. David and C. H. Nicholas, *J. Chem. Phys.* **109**, 10180 (1998).
- <sup>63</sup>J. Akola, M. Manninen, H. Hakkinen, U. Landman, X. Li, and L.-S. Wang, *Phys. Rev. B* **60**, R11297 (1999).
- <sup>64</sup>M. Ohara, K. Miyajima, A. Pramann, A. Nakajima, and K. Kaya, *J. Phys. Chem. A* **106**, 3702 (2002).